JARO 20: 461–474 (2019)
DOI: 10.1007/s10162-019-00734-2

JARO
Journal of the Association for Research in Otolaryngology

Research Article

Morphological Immaturity of the Neonatal Organ of Corti and Associated Structures in Humans

Sebastiaan W. F. Meenderink,[1] Christopher A. Shera,[1,2] Michelle D. Valero,[3] M. Charles Liberman,[3,4] and Carolina Abdala[1]

[1]*Auditory Research Center, Caruso Department of Otolaryngology, University of Southern California, 1640 Marengo Street, Los Angeles, CA 90033, USA*

[2]*Department of Physics and Astronomy, University of Southern California, Los Angeles, CA 90089, USA*

[3]*Eaton-Peabody Laboratories, Massachusetts Eye and Ear, 243 Charles Street, Boston, MA 02114, USA*

[4]*Department of Otolaryngology, Harvard Medical School, Boston, MA 02115, USA*

Received: 15 May 2019; Accepted: 18 July 2019; Online publication: 12 August 2019

ABSTRACT

Although anatomical development of the cochlear duct is thought to be complete by term birth, human newborns continue to show postnatal immaturities in functional measures such as otoacoustic emissions (OAEs). Some of these OAE immaturities are no doubt influenced by incomplete maturation of the external and middle ears in infants; however, the observed prolongation of distortion-product OAE phase-gradient delays in newborns cannot readily be explained by conductive factors. This functional immaturity suggests that the human cochlea at birth may lack fully adult-like traveling-wave motion. In this study, we analyzed temporal-bone sections at the light microscopic level in newborns and adults to quantify dimensions and geometry of cochlear structures thought to influence the mechanical response of the cochlea. Contrary to common belief, results show multiple morphological immaturities along the length of the newborn spiral, suggesting that important refinements in the size and shape of the sensory epithelium and associated structures continue after birth. Specifically, immaturities of the newborn basilar membrane and organ of Corti are consistent with a more compliant and less massive cochlear partition, which could produce longer DPOAE delays and a shifted frequency-place map in the neonatal ear.

Correspondence to: Carolina Abdala · Auditory Research Center, Caruso Department of Otolaryngology · University of Southern California · 1640 Marengo Street, Los Angeles, CA 90033, USA. Telephone: 323 865-1281; email: carolina.abdala@usc.edu

Keywords: Temporal bone, Cochlea, Newborn, Development, OAE, Anatomy, Basilar membrane

INTRODUCTION

Development of Human Cochlear Anatomy

The study of human cochlear development has focused on hair cell differentiation and innervation, hair-bundle development and organization, morphogenesis of the tectorial membrane, and maturation of the stria vascularis (Tanaka et al. 1979; Igarashi and Ishii 1980; Sánchez-Fernández et al. 1983; Pujol 1985; Pujol and Lavigne-Rebillard 1985; Lavigne-Rebillard and Pujol 1986, 1987, 1988; Lavigne-Rebillard and Bagger-Sjöbäck 1992; Lim and Rueda 1992). Many reports have also described gross developmental gradients, such as the maturation of the cochlear base before the apex, the maturation of inner before outer hair cells, and the innervation of sensory cells by afferent before efferent nerve fibers (e.g., Retzius 1884; Bast and Anson 1949; Bredberg 1968; Pujol and Hilding 1973).

Collectively, this anatomical work has established that the human cochlea is fully coiled by the 9th embryological week (Pujol and Lavigne-Rebillard 1985), though growth and elongation of the cochlear segment of the labyrinth continue through 17–19 gestational weeks, when it attains adult-like dimensions (Jeffery and Spoor 2004). By around 9–10 weeks,

afferent nerve fibers enter the undifferentiated epithelia of the otocyst. Two weeks later, hair cells can be clearly distinguished (at least in the basal half of the cochlea; outer hair cells are not yet recognizable in the apex). Both afferent and efferent inner hair cell (IHC) patterns of innervation are nearly adult-like by the 14th gestational week; however, arrival of the medial efferent endings on the outer hair cells (OHCs) occurs much later (20–22 weeks) (Pujol 1985). Stereocilia formation begins on the IHCs by 11–12 weeks and a week or so later on OHCs. The stereocilia rapidly become appropriately graded in length, and the tip and lateral links are observable. However, not until 20–22 fetal weeks does an adult-like pattern of stereocilia form on OHCs (Igarashi 1980). The shape and innervation of the OHC also remain immature longer than that of the IHC; it assumes its characteristic elongated shape about the time that the large efferent synapses are formed, though post-synaptic specializations remain immature into the third trimester. The time point by which sensory cells of the *human* cochlea reach their terminal mitosis has not been well defined, but in other mammals, this milestone occurs early in gestation. For the basal mouse cochlea, sensory cells are postmitotic by embryological days 15–16 (Ruben 1967; Roberson and Rubel 1994; Lim and Brichta 2016).

In general, these anatomical studies indicate that the micromechanical elements of morphology giving rise to active cochlear processes are mostly complete by the end of the second trimester although changes to outer hair cells and their efferent innervation continue into the 3rd trimester.

Development of Human Cochlear Function

Over the last several decades, otoacoustic emissions (OAEs) have provided a tool for investigating the *functional* development of the human cochlea. However, immaturities in the acoustics of the newborn ear canal and anatomy of the middle ear, both of which are developing in early infancy, can confound OAE interpretation (see Abdala and Keefe 2012). An exception to this is the phase of the cubic ($2f_1 - f_2$) distortion-product OAE (DPOAE), which is not impacted by changes in the stimulus level over the range used for most measurements ($L_1 = 45$ to 65 dB SPL; Abdala et al. 2011a). This makes DPOAE phase a particularly useful feature to gauge cochlear status in newborns without contamination from immaturities of the outer and middle ear.

DPOAE phase has been used as a noninvasive tool for assessing deviations from cochlear scaling symmetry in newborns and adults. In laboratory animals, deviations from perfect scaling are evident in the widths and shapes of neural tuning curves. Although tuning curves vary only slowly with characteristic frequency (CF) in the basal half of the cochlea, consistent with approximate local scaling, the variations become much more pronounced in the apical half (e.g., Temchin et al. 2008). When the cochlear tonotopic map is exponential, scaling implies that excitation patterns produced by tones of different frequencies are simply translated along the basilar membrane such that traveling waves accumulate the same phase regardless of where they peak along the cochlear partition (Zweig 1976). In the fixed-ratio DPOAE paradigm, the two stimulus frequencies (f_1 and f_2) used to evoke the DPOAE are changed while their ratio (f_2/f_1) is held constant. At or near an optimal ratio of 1.2, DPOAE phase remains approximately invariant across much of the frequency range, consistent with a scaled cochlea (Shera et al. 2000). However, for f_2 frequencies below approximately 1–2 kHz, the phase of the distortion emission begins to increase as frequency decreases. The emergence of this non-zero phase slope is consistent with the existence of a mid-cochlear break in scaling within the human cochlea analogous to that seen in laboratory animals.

Although the location of this "break" frequency does not change during the human lifespan (Abdala et al. 2011b; Abdala and Dhar 2012), the slope of DPOAE phase below the break frequency does—newborns have a significantly steeper low-frequency slope than adults and a correspondingly longer phase-gradient delay by nearly 1 ms. This OAE immaturity cannot easily be attributed to the immature middle ear, both because the prolonged delay is too long to result from middle-ear transmission and because the phases of distortion-type emissions are largely insensitive to variations in the effective stimulus level entering the cochlea (Abdala et al. 2011a). Thus, prolonged DPOAE delays appear to indicate residual immaturities in the newborn cochlea. This hypothesis—that the non-adult-like DPOAE phase observed in newborns arises from immature geometry or material properties of the neonatal cochlear partition—provides the impetus for the current study.

Although the microanatomy of the developing cochlea has been well defined and appears to develop mostly in utero, no quantitative comparison of the architecture of the newborn and adult cochlea has been undertaken. The present study fills this void. Properties that control the mass and stiffness gradient of the basilar membrane and organ of Corti dictate the passive cochlear vibration defined by von Békésy (1960) and establish the tonotopic map. We

hypothesize that immaturity of structure in the newborn cochlea could produce a non-adult-like tonotopic map along the cochlear partition, in particular in its apical half.

MATERIALS AND METHODS

Temporal Bones

In this study, we evaluated the anatomy of human temporal bones from the collection at Massachusetts Eye and Ear (MEE). The temporal bones were prepared for light microscopy by standard techniques involving fixation, decalcification, celloidin-embedding, 20-μm horizontal sectioning, and hematoxylin and eosin staining of every 10th section (Merchant and Nadol 2010). The temporal bones were selected from a subset of cases previously screened for normalcy, image quality, and post-mortem autolysis (Makary et al. 2011; Amatuzzi et al. 2011). The adult temporal bone samples were from 17 individuals ranging from 17 to 58 years with a mean age of 40 years. Infant temporal bone samples were from 30 newborns, including 11 premature neonates born between 26 and 34 weeks gestational age (mean = 30 weeks) and 19 full-term neonates born at a mean gestational age of 40 weeks. The newborns survived for a mean of 4 weeks after birth and suffered to varying degrees from clinical conditions such as hypoxia, meconial aspiration, and sepsis (see Amatuzzi et al. 2011 for details). Because initial analysis of the data revealed no differences between term and preterm newborns, and because the data at each post-conceptional age were insufficient to form a maturational continuum, the two infant subgroups were combined for analyses.

Using differential interference contrast optics, we obtained images of mid-modiolar sections, which include up to five cross-sections of the cochlear duct that roughly correspond to tonotopic frequencies of 3.5, 1.2, 0.75, 0.28, and 0.15 kHz. These estimates are derived by converting the distance from the cochlear base in a standard 2-D cochlear reconstruction (e.g., Fig. 1.60 in Schuknecht's *Pathology of the Ear*; Merchant and Nadol 2010) to frequency using the Greenwood map for the human cochlea (Greenwood 1990). By measuring all cochlear turns using one mid-modiolar section, we could not ensure an exactly orthogonal sectioning angle for all cochlear locations. In any given half-turn, deviations from an orthogonal sectioning angle affect measurements that include a radial dimension (e.g., basilar membrane or scalae width) but do not affect measurements in the opposite direction (e.g., organ of Corti height).[1] Errors in section selection will produce the largest effects in the apical turn, where the radius of the arc is smallest and the angular deviation of the sectioning angle from 90° could be the greatest. We can use geometry to estimate the possible magnitude of such effects: In the apical turn (where the typical radius is ~1 mm), even an "error" in section selection as large as ±20% translates into only a ± 6% error in measured basilar membrane width; in the basal turn, the error would be only ±3%. Importantly, there is no evidence that these errors would be age specific. All images were processed by manually mapping the positions of various anatomical structures, as detailed below, using the software package Fiji (Schindelin et al. 2012).

Measurements

Cochlear Scalae For each temporal bone, a low-magnification image (×2 objective; 0.23 pixel/μm) captured multiple cross-sections through the endolymphatic (scala media) and perilymphatic spaces (scala tympani and scala vestibuli) of the cochlear duct. Polygons outlining the perimeters of the scalae for each cross-section are superimposed in Fig. 1a. Each polygon traces the boundary between the fluid-filled lumen and the lining epithelium. To outline the scala tympani (*green* in Fig. 1a), we followed the "underside" of the organ of Corti (OoC). With this convention, the OoC is excluded from the scala tympani although electrochemically it is within the perilymphatic space (Tasaki et al. 1954). On the other side of the OoC, the polygon outlining the scala media (*blue*) ignores the inner spiral sulcus and follows a straight line from the tip of the limbus to the estimated location of the inner hair cells. Finally, we approximated Reissner's membrane, which separates scala media and scala vestibuli (*red*), as a straight line between its contacts at the limbus and the spiral ligament. We used the polygons to calculate the areas of the different scalae using Gauss's area formula. In addition to these polygons, we used a straight line-segment (*black*, Fig. 1a) to estimate the orientation of the spiral lamina for each cochlear cross-section relative to the mid-modiolar axis. The outlines of the

[1] The sectioning angle could also be off-orthogonal in the other direction (i.e., in the direction which would elongate the organ of Corti height rather than the BM width). However, we are confident that we are safe on that score, because the factor controlling that angle is the tilt of the modiolar axis with respect to the horizontal (see Figure 8). If we were "off" in the neonates, the different turns would not appear concentric in 2D reconstructions. Although we did no 2D reconstructions for the present study, the Liberman lab has completed two prior studies of human neonatal cochleae prepared by standard celloidin techniques and can verify that the spirals were just as concentric in the neonatal 2D reconstructions as in the adults.

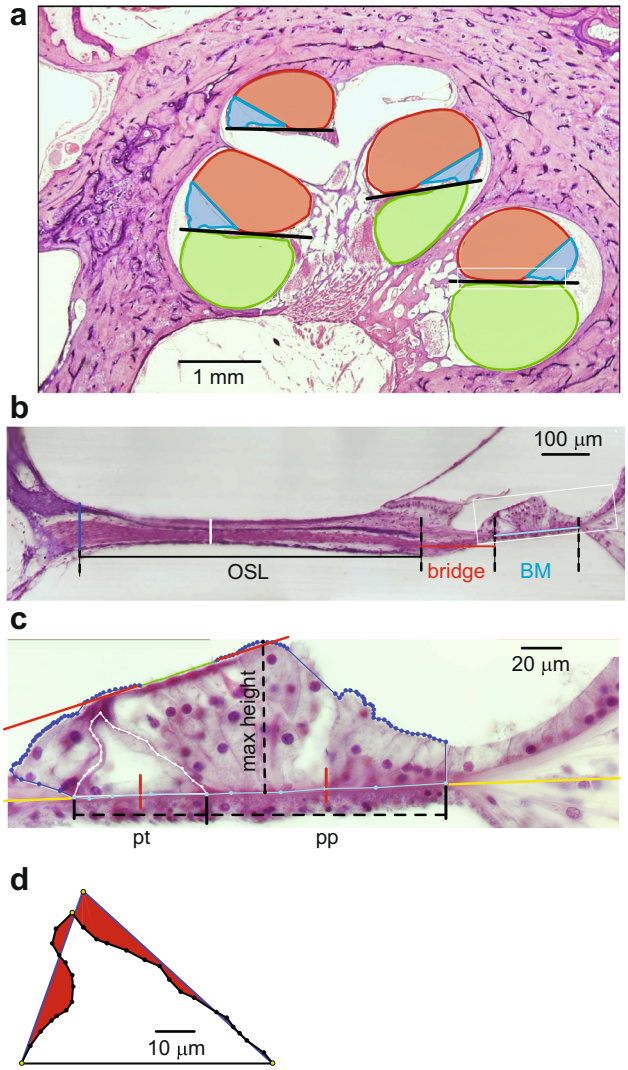

FIG. 1. Description of the measurements. **a** Image of a mid-modiolar, cochlear section from the left ear of an adult case. For each cross-section of the cochlear duct, the orientation of spiral lamina was approximated by a straight line (*black*), and the outlines of scala tympani (*green*), scala media (*blue*), and scala vestibuli (*red*) were described with polygons. Scale bar corresponds to 1 mm. **b** Composite image showing the entire cochlear partition from the basal turn in **a**. The partition consists of the spiral lamina and the BM. The spiral lamina includes an ossified portion (OSL) and a non-ossified portion, recently dubbed the "bridge" (Raufer et al. 2019). Scale bar, 100 μm. **c** Composite image showing the organ of Corti (OoC) from the basal turn in **a**. The outline of the OoC was described by a polygon (*blue*) that included the basilar membrane (BM; *cyan*) and the reticular lamina (RL; *green*) in the outer hair cell region. The BM consists of pars pectinata (*pp*) and pars tecta (*pt*), which are separated by the center of the outer pillar cell foot. The thickness ("height") of BM was measured at two locations corresponding to the midpoints of pp and pt (*vertical red lines*). Both the BM and RL were fit with straight lines (*yellow* and *red*, respectively). The polygon outlining the OoC was also used to obtain the maximum OoC height (*vertical black dashed line*). The outline of the tunnel of Corti (ToC) was described by a polygon (*white*) that followed the inner and outer pillars. The scale bar corresponds to 20 μm. **d** The polygon describing the ToC (*black*) was used to calculate a deformation index. For this, the sides of the polygon were straightened out to form a triangle (*blue*). The areas between the polygon and this triangle were calculated (*red*), and the sum of these areas was divided by the area of the triangle. In this example, the deformation index is 0.2. Scale bar, 10 μm

scalae in Fig. 2A have been rotated so that the spiral lamina is oriented horizontally.

Spiral Lamina and Bridge Using a ×20 objective (2.25 pixel/μm), we imaged the cochlear partition, which divides scala vestibuli from scala tympani and comprises the spiral lamina and basilar membrane, at each cochlear location in multiple, partially overlapping images. At each location, the overlapping images were joined using the Fiji plugin "Stitching" (Preibisch et al.

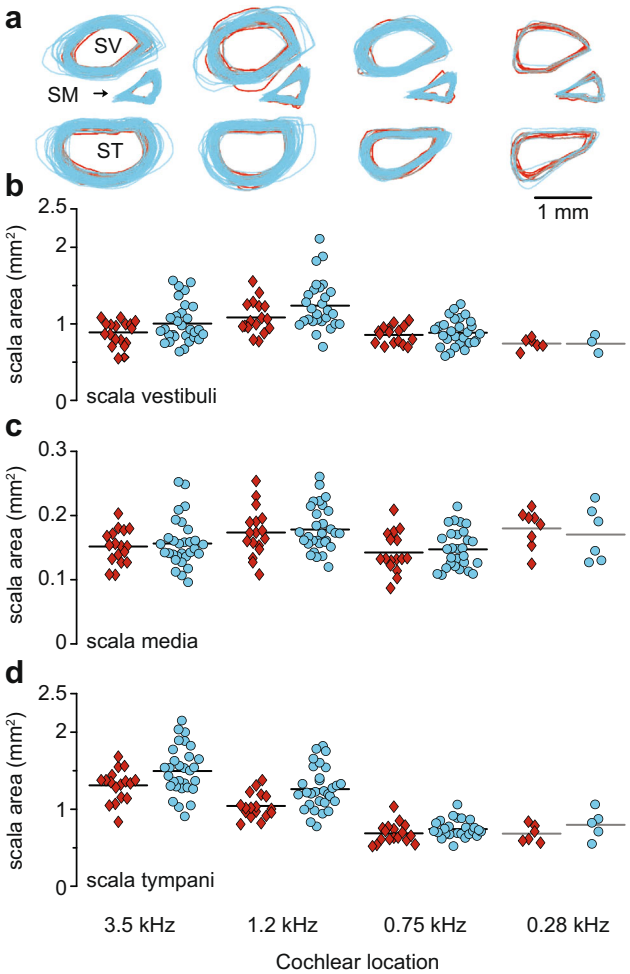

FIG. 2. Size and shape of cochlear scalae in adults versus newborns. (A) Overlays of the polygons describing the three scalae (*SV* = scala vestibuli; *SM* = scala media; *ST* = scala tympani) for adults (*red*) and newborns (*cyan*). The outlines are arranged in four columns that represent different cochlear locations, see the abscissa in (D). Outlines are oriented with the modiolus to the left, aligned on their centroids, and rotated so that the spiral lamina runs horizontally (see also Fig. 1a). The offsets between the different scalae are arbitrary and were chosen for visual clarity. The scale bar (1 mm) applies to all outlines. Scatter plots for the areas of (B) scala vestibuli, (C) scala media, and d scala tympani in the different cross-sections of the cochlear duct for adults (*red diamonds*) and newborns (*cyan circles*). The areas were obtained from the polygons using Gauss's area formula. Data are grouped according to cochlear location. Horizontal bars indicate mean values. *Gray* horizontal bars indicate that the cochlear location was excluded from statistical analysis due to insufficient observations ($N < 8$)

2009) to show the entire partition (Fig. 1b). The spiral lamina is ossified near the modiolus, and the ossification extends progressively farther out towards the BM as the spiral progresses from apex to base. The (distal) non-ossified portion of the lamina, nearest the BM, has recently been dubbed the "bridge" (Raufer et al. 2019).

To measure the width of the osseous spiral lamina (OSL), we defined the distal endpoint as whichever of its bony shelves extended farthest from the modiolus. On the modiolar side, we defined the initial point as follows: we first identified the minimal OSL thickness (vertical white line in Fig. 1c) and then found the point closest to the modiolus at which the thickness was twice the minimum (vertical blue line in Fig. 1c). We also measured the width of the non-ossified spiral lamina (the "bridge") as the distance between the distal end of the OSL and the proximal end of the BM.

Basilar MembraneA third set of tiled images (× 100 oil-immersion objective; 11.36 pixel/μm) was stitched to visualize the OoC cochlear partition (Fig. 1c). In each case, the width of the basilar membrane (BM) was obtained using a polyline (*cyan*) from the center of the foot of the inner pillar cell on the modiolar side to the basilar crest on the side of the spiral ligament. The center of the outer pillar foot served as a landmark separating the BM into two adjoining segments: pars tecta (pt; inner pillar to outer pillar) and pars pectinata (pp; outer pillar to basilar crest). The widths of these two BM segments sum to the total width of the BM. The thickness (or height) of the BM was measured at the midpoints of pt and pp (*vertical red line segments*).

Organ of Corti In the same stitched image (Fig. 1c), a second polyline (*blue*), continuous with the polyline defining the BM, traces the boundary of the OoC. To define the reticular lamina (RL), we used the polyline's vertices located over the apical aspects of the outer hair cells (*green*); these points were fit by a straight line (*red*). The slope of this line was compared to the slope of the straight line fit to the BM vertices (*yellow*) beneath the RL to obtain the angle between the RL and the BM. The combined polygon (*cyan* + *blue*) was used to calculate the total OoC area and determine the maximum OoC height (*dashed black line*). The latter was taken as the largest orthogonal distance between the BM and the upper margin of the OoC. Finally, we used a polygon to describe the tunnel of Corti (ToC; *white*).

Tunnel of Corti Within the sensory epithelium, the two rows of pillar cells form the tunnel of Corti (ToC). These cells are thought to form a semi-rigid structure, coupling BM vibrations to the hair cell stereocilia (Dallos 2003). We delineated the ToC in each cochlear cross-section with a polygon and used this to quantify the degree of compression (see Fig. 1d). After correction for compression artifacts, the ToC forms a triangle defined by four parameters: (1) its width at the base, (2) its height, (3) the angle at its apex, and (4) its skewness. The latter locates the apex relative to the base and varies between −1 (apex directly over the foot of the outer pillar cell) and +1 (apex directly over the foot of the inner pillar cell). A skewness of 0 indicates a symmetrical, equilateral triangle.

Analysis

As a result of post-mortem autolysis and subsequent tissue removal and preparation, artifacts can occur (e.g., Edge et al. 1998). One of their most prominent is a partial collapse of the tunnel of Corti (ToC), in which one or both pillar cells appear to buckle. To quantify this effect for each cross-sectional image, we used the polygon that describes the (buckled) ToC to calculate a "deformation index," as illustrated in Fig. 1d. For this, the sides of the polygon were straightened without changing their lengths to form a triangle (*blue*). The deformation index is defined as the total area between the polygon and this triangle (*red*), normalized by the area of the triangle. The deformation index is 0 for an uncollapsed ToC and increases with the amount of buckling. The results could have been confounded by compression artifacts if they differed systematically with age and/or cochlear location. To address this possible confound, we analyzed the deformation index and found no effect of age ($F(1,132) = 0.36$, $p = 0.71$) or cochlear location ($F(3,132) = 0.36$, $p = 0.55$) and no significant interaction ($F(3,132) = 1.28$, $p = 0.28$). This suggests that compression effects, when present, did not exert a systematic bias on our results. We also recognize that fixed material is dehydrated and will provide artificially thinner measures of tissue height, for example (Edge et al. 1998); however, it is unlikely that this inevitable fixation artifact impacted the newborn more than the adult tissue.

The image analyses yielded 18 metrics for each cochlear location (see Table 1), although not all metrics could be determined for all temporal bones and/or locations. In most mid-modiolar sections, the scalae in the apical-most turn were in direct communication, due to the presence of the helicotrema within the cutting plane (e.g., Fig. 1a). In those regions, the scala perimeter was not measured. Also, when the OoC at a given cochlear location included many ruptured cells or a collapsed ToC, the area and height of the OoC were not measured. If the OHC region was damaged, an estimate of the angle between the RL and the BM was also omitted. In some cases, the BM boundaries were unclear, and

TABLE 1

For each temporal bone, 18 morphological metrics were obtained. The columns labeled "age" and "cochlear location" give the *F*-statistic, within-factor, and error degrees of freedom (in parentheses) and the corresponding *p* values for the main effects from two-way ANOVAs. Significance ($p < 0.05$) is indicated by *gray shading* of the cells

				Age		Cochlear Location	
				F	*p* value	*F*	*p* value
1	area of scala	scala vestibuli (SV)		5.82 (1, 130)	0.017	17.9 (2, 130)	1.4e-7
2		scala media (SM)		0.62 (1, 132)	0.43	9.59 (2, 132)	1.3e-4
3		scala tympani (ST)		14.4 (1, 130)	2.2E-4	98 (2,130)	1.1e-26
4	bridge width			19 (1, 86)	3.6e-5	51.2 (2, 86)	2.2e-15
5	osseous spiral lamina width (OSL)			0.077 (1, 86)	0.78	65.7 (2, 86)	4.8e-18
6	basilar membrane (BM)	pars pectinata (pp)	width	9.27 (1, 160)	2.7e-3	366 (4, 160)	2.3e-79
7			thickness	16.2 (1, 148)	1.3e-4	23.8 (2, 82)	7.1e-9
8		pars tecta (pt)	width	5.5 (1, 160)	0.02	32.5 (4, 160)	8.4e-20
9			thickness	5.41 (1, 82)	0.022	8.93 (3, 104)	2.6e-5
10		total width (pp + pt)		14.2 (1, 160)	2.3e-4	404 (4, 160)	1.8e-82
11	total width (OSL + BM + bridge)			12.4 (1, 93)	6.6e-4	2.7 (2, 93)	0.072
12	organ of Corti (OoC)	maximum height		81.7 (1, 127)	2.3e-15	12.2 (3, 127)	4.5e-7
13		area		53.8 (1, 127)	2.3e-11	21.9 (3, 127)	1.8e-11
14		angle between RL and BM		10.3 (1, 148)	1.6e-3	5.32 (4, 148)	5e-4
15	tunnel of Corti (ToC)	width		11.9 (1, 133)	7.4e-4	57.6 (3, 133)	6.5e-24
16		height		120 (1, 133)	3e-20	15.9 (3, 133)	7.2e-9
17		angle at apex		95.3 (1, 133)	2.7e-17	1.26 (3, 133)	0.29
18		skewness		14.7 (1, 133)	1.9e-4	7.43 (3, 133)	1.2e-4

measurements were not made. In general, the OoC was more disorganized in the apical turn; consequently, the number of observations decreases towards the apex.

The results detailed below describe the distributions and central tendencies for these 18 metrics and examine newborn-adult differences in cochlear morphology, as well as differences across cochlear location in both age groups. The effects of age and cochlear location on each metric were assessed using two-way ANOVAs (MATLAB). Although all data points are shown in the scatter plots, any location with fewer than eight observations in either age category was excluded from all statistical analyses and comparisons. Throughout the manuscript, we use $p < 0.05$ to indicate significance.

The two-way ANOVAs conducted on these individual metrics showed no significant interaction between age and cochlear location, except for BM thickness (pars tecta only). Hence, we consider the main effects of age and cochlear location on each metric independently. Because the primary aim of this study was a comparison between newborn and adult cochleae, we first present the main effects of age on each metric

and the effects of cochlear location follow. Table 1 provides a summary of the statistical results.

RESULTS

Age Effects

Cochlear Scalae Figure 2A shows superimposed outlines of all adult and infant scalae, grouped by cochlear location. Qualitatively, newborn scalae appear slightly larger than those in adults. Scala areas calculated from these outlines are shown as scatterplots in Fig. 2B–D. A two-way ANOVA (age × cochlear location) found an age effect on the scala area for both scala vestibuli and scala tympani, with larger areas measured in newborns compared to adults; this is evident in the mean area values provided in Table 2 (rows 1 and 3) and the scatter plots of Fig. 2 (horizontal lines display mean values). The area of scala media was not significantly different between age groups at any cochlear location (also evident in Table 2, row 2).

Spiral Lamina Widths The spiral lamina is ossified near the modiolus, and the ossification extends progressively farther towards the BM when progressing down the spiral from apex to base. The (distal) non-ossified portion of the lamina, nearest the BM, has been dubbed the "bridge," and has shown to undergo sound-induced vibrations similar to that seen in the pars tecta of the BM (Raufer et al. 2019). Measurements of the bridge width (Fig. 3) reveal an age effect, as newborns had a wider bridge segment

TABLE 2

Mean values (top) and numbers of observations (below) for the 18 morphometric features in adult and newborn (newbn) specimens; *SV* scala vestibuli, *SM* scala media; *ST* scala tympani; *OoC* organ of Corti; *RL* reticular lamina; *BM* basilar membrane; *OSL* osseous spiral lamina; *ToC* tunnel of Corti

		3.5 kHz		*1.2 kHz*		*0.75 kHz*		*0.28 kHz*		*0.15 kHz*	
		Adult	*Newbn*	*Adult*	*Newbn*	*Adult*	*Newbn*	*Adult*	*Newbn*	*Adult*	*Newbn*
1	SV area (mm^2)	0.9 17	1.02 30	1.1 17	1.25 28	0.87 16	0.9 28	0.76 6	0.75 3	–	–
2	SM area (mm^2)	0.15 17	0.16 30	0.17 17	0.18 30	0.15 16	0.15 28	0.18 8	0.17 6	–	0.12 1
3	ST area (mm^2)	1.31 17	1.5 30	1.05 17	1.27 30	0.69 17	0.75 25	0.69 6	0.8 5	–	–
4	Bridge width (µm)	228.6 13	258.1 22	304.4 14	333.7 16	334.6 11	415.7 16	413.5 3	499.2 5	–	–
5	OSL width (µm)	726.6 13	728.9 22	538.2 14	576.5 16	429.4 11	407.1 16	318.95 3	335.9 5	–	–
6	BM, pp width (µm)	131.5 14	145.1 28	173.6 15	182.5 23	231.1 15	248.5 26	305.8 8	321.7 18	387.6 9	402.9 14
7	BM, pp thick (µm)	1.92 13	1.7 21	1.31 11	0.89 10	1.4 12	0.81 21	0.53 4	0.74 6	0.53 1	0.83 7
8	BM, pt width (µm)	70.39 14	74.95 28	85.08 15	92.42 23	91.22 15	93.1 26	94.75 8	99.31 18	87.59 9	87.13 14
9	BM, pt thick (µm)	1.26 11	0.94 24	1.11 8	1.01 16	0.77 11	0.82 21	0.99 8	0.89 13	0.89 7	0.72 5
10	BM tot. width (µm)	201.9 14	220.1 28	258.7 15	274.9 23	322.3 15	341.6 26	400.6 8	421 18	475.2 9	490 14
11	OSL + BM + bridge (µm)	1156 13	1207 24	1104 15	1188 16	1075 13	1167 18	1158 5	1217 8	–	–
12	OoC height (µm)	66.02 14	45.6 23	76.78 15	60.65 21	73.41 15	54.63 24	79.86 7	62.01 17	62.69 9	42.3 14
13	OoC area ($\times 10^4$ μm^2)	0.98 14	0.68 23	1.31 15	1.01 21	1.32 15	0.97 24	1.51 7	1.17 17	1.23 9	1.09 14
14	Angle RL re BM (deg)	14.39 14	8.81 22	15.53 15	14.15 21	15.76 15	11 24	15.19 8	12.47 16	8.69 9	7.77 14
15	ToC width (µm)	69.66 14	74.2 28	84.94 14	92.78 22	90.39 15	93.1 25	94.09 8	99.17 15	89.85 5	90.72 11
16	ToC height (µm)	39.41 14	30.39 28	46.87 14	37.36 22	44.97 15	35.11 25	49.15 8	36.64 15	44.07 5	32.21 11
17	ToC angle (deg)	78 14	97.08 28	77.07 14	95.79 22	82.65 15	98.85 25	80.55 8	98.59 15	85.38 5	101.7 11
18	Skewness	0.45 14	0.28 28	0.53 14	0.43 22	0.53 15	0.45 25	0.52 8	0.48 15	0.46 5	0.43 11

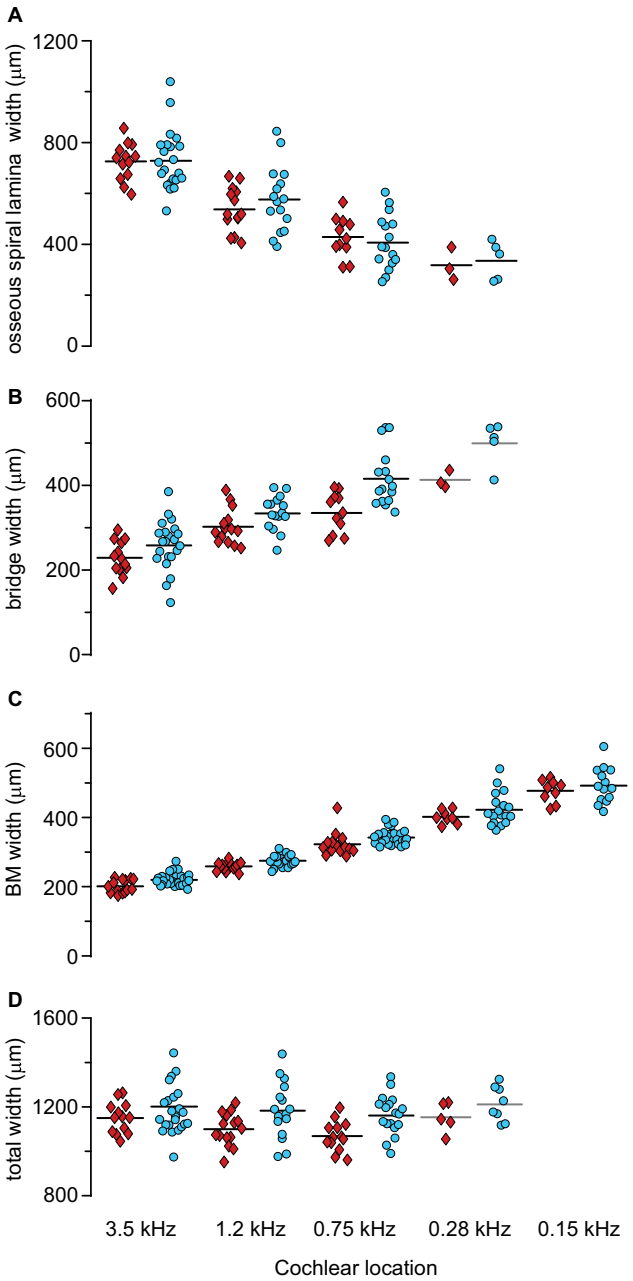

FIG. 3. Widths of the three segments of the cochlear partition. Scatter plots for the widths of (A) the osseous spiral lamina, (B) the bridge, (C) the basilar membrane (pt + pp), and (D) the complete cochlear partition (OSL + bridge + BM) in newborns (*cyan circles*) and adults (*red diamonds*) grouped by cochlear location

than adults by between 30 and 81 μm (~10–24 %) across cochlear location; no such age effect was noted for osseous spiral lamina width (see mean values in Table 2, row 5). Also, in both age groups, the width of the bridge covaries with that of the BM and therefore with cochlear location (see Fig. 4).

Basilar Membrane Passive mechanical properties of the BM (e.g., its stiffness) play a role in shaping the tonotopic map along the cochlear spiral. We hypothesized that newborn-adult differences in

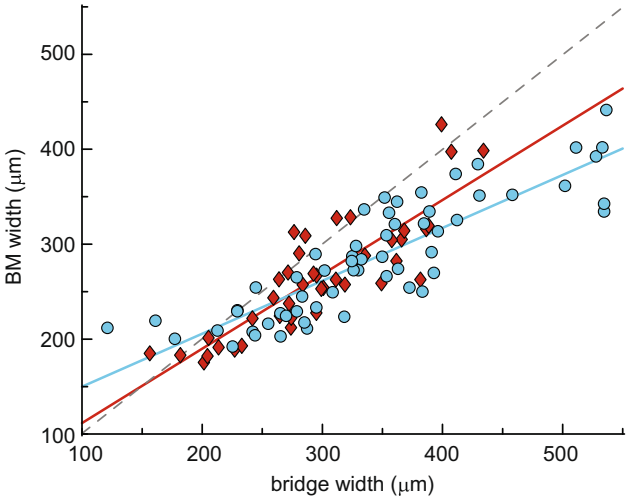

FIG. 4. Correlation between bridge width and basilar-membrane width. Scatter plot of bridge width versus basilar membrane (BM) width for newborns (*cyan circles*) and adults (*red diamonds*), with straight-line fits ($W_{BM} = A\ W_{bridge} + B$) to the data. The best-fitting parameter values (with respective 95% confidence intervals in parentheses) are as follows: newborn $A = 0.56$ (0.47–0.64), $B = 94$ (64–125) μm ($r^2 = 0.75$); adult $A = 0.78$ (0.63–0.94), $B = 33$ (−14–80) μm ($r^2 = 0.73$). The *gray dashed line* indicates equality

DPOAE phase-gradient delays might reflect underlying differences in the mechanical properties of the BM. We measured the width and the thickness of both the pars pectinata (pp) and pars tecta (pt), the two adjoining segments of the BM. The endpoints of the basilar membrane used to measure width are somewhat arbitrary. Given the large total width of the BM, however, small uncertainties (on the order of a few pixels) in estimating these two points contribute only marginally. Therefore, the considerable spread in the measures of BM width likely reflects natural variation rather than measurement errors. Both pp and pt show age effects (Fig. 5A, B) and are wider in infants than in adults at each cochlear location (see Table 2, rows 6 and 8). Consequently, the total BM is also wider in newborns than adults with an overall mean difference of 17.8 μm (~6%) between the two age groups (Table 2, row 10).

The scatter plots in Fig. 5C and D show the thickness (or height) of each BM segment (pp and pt) as a function of cochlear location. Because the BM thickness spans only a few tens of pixels in the images we utilized, an error of even a few pixels can significantly affect the estimated value. Indeed, quantization of the thickness values is evident in Fig. 5C and D. However, such measurement errors cannot account for the systematic differences observed between age groups. Moreover, BM thickness varies considerably in the radial direction at all cochlear locations, and this inherent variation further masks potential measurement errors. Additionally, our adult measures of BM thickness values shown in Fig. 5 are

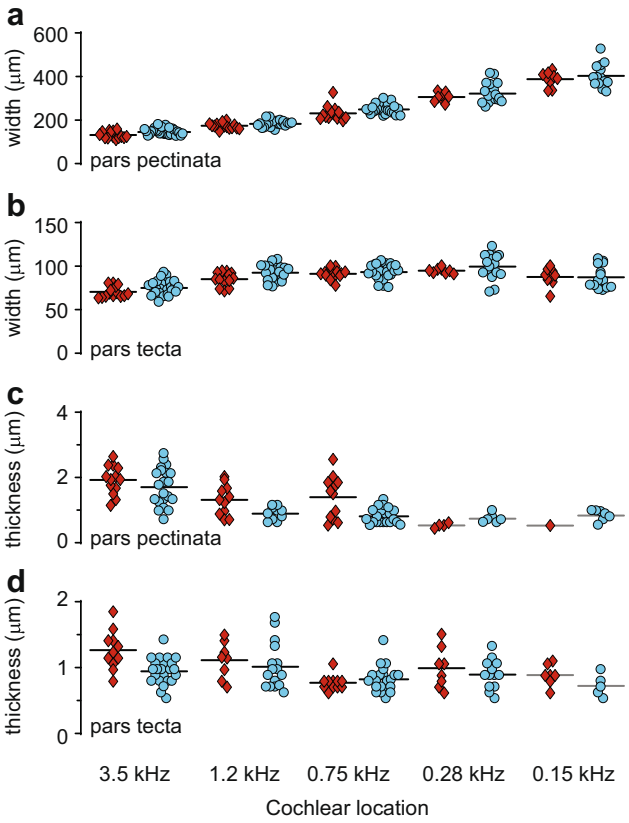

FIG. 5. Width and thickness of the basilar membrane in adults versus newborns. Scatter plots for the width (A, B) and thickness (C, D) of pars pectinata and pars tecta, respectively. Data from adults are shown as *red diamonds* and newborns as *cyan circles*, while mean values are indicated by horizontal bars. The data are grouped according to cochlear location as indicated along the abscissa in (D). *Gray* horizontal bars indicate that the data were excluded from statistical analysis due to insufficient observations ($N < 8$) at that cochlear location

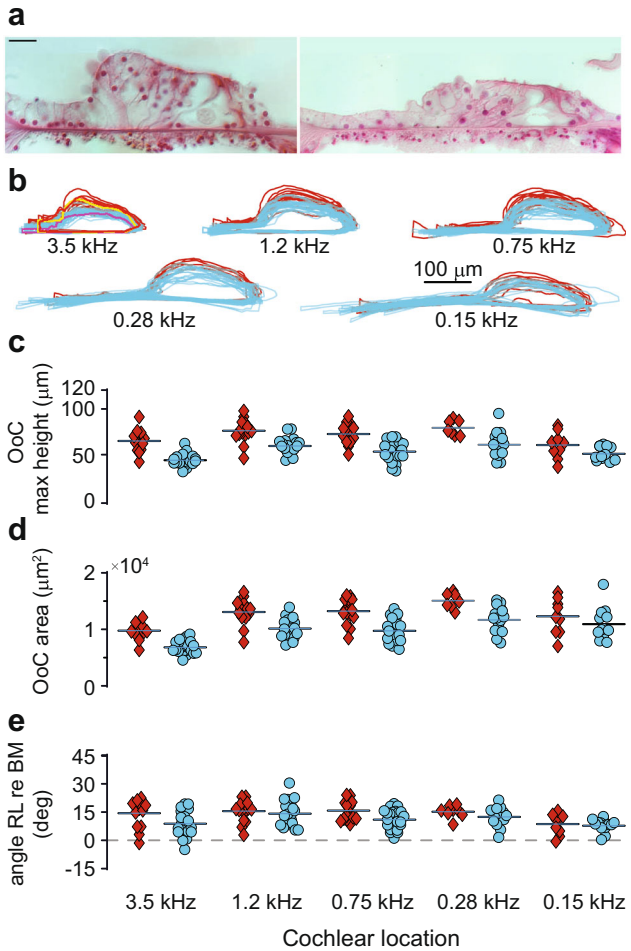

Fig. 6. Size and shape of the organ of Corti in adults versus newborns. (A) Composite images of the organ of Corti (OoC) for an adult (*left*) and a newborn (*right*) from the base of the cochlea (3.5 kHz). (B) Superimposed outlines of the OoC for adults (*red*) and newborns (*cyan*) for cross-sections at the five cochlear locations. Outlines are oriented with the modiolus to the left, aligned on their centroids, and rotated so that the basilar membrane runs horizontally. The *yellow* and *magenta* outlines are for the adult and newborn images in (A), respectively. The scale bar (100 μm) applies to all outlines. Scatter plots for (C) the maximum OoC height, (D) the area of the OoC, and (E) the angle between reticular lamina and basilar membrane. In the scatter plots, data are clustered by tonotopic location as indicated in abscissa (F). Adult data are shown as *red diamonds* and newborn data as *cyan circles*. Horizontal bars indicate mean values. *Gray* horizontal bars indicate that the cochlear location was excluded from statistical analysis due to insufficient observations ($N < 8$)

quantitatively and qualitatively similar to those previously described (Bhatt et al. 2001).

We found the pars pectinata to be significantly thinner in newborns than in adults (see Table 2, row 7). For pars tecta thickness, there was a marginal but significant interaction between age and cochlear location ($F(3,111) = 2.91$, $p = 0.04$). With the exception of the 0.75-kHz cochlear location, which likely produced the significant interaction (see Fig. 5D), pars tecta is also thinner in newborns than in adults by an average of 0.17 μm (~15 %; Table 2, row 9).

Organ of Corti Figure 6A shows stitched images of the OoC from the basal turn (cochlear location = 3.5 kHz) for an adult (left) and a term newborn (right). In the newborn cochlea, the region of the OoC occupied by Hensen cells is less pronounced than it is in the adult cochlea, giving the neonatal OoC a flatter appearance. This difference exists throughout most of the cochlea as noted by the superimposed outlines shown in Fig. 3B. Figure 6C–E confirm this observation, showing scatter plots for the three metrics used to describe OoC shape. An ANOVA applied to each measure indicates differences between newborns and adults: newborns have a flatter OoC corresponding to a reduced maximum OoC height and a reduced total OoC area (Fig. 6C and D; Table 2, rows 12 and 13). The less pronounced Hensen cell area makes the RL run more parallel to the BM in newborns compared to adults, as quantified by the reduced angle between the two (Fig. 6E, Table 2, row 14).

Tunnel of Corti Although measured independently, the width of the ToC (Fig. 7A) matches the width of pars tecta, as expected (see Fig. 5B), and is wider in newborns than in adults as shown by the mean values in Table 2 (row 15). Because the newborn OoC is flatter than that of adults (see Fig. 6), it is not surprising that ToC height also shows a significant effect of age with a shorter ToC observed in the newborn ear by an average of 10 μm (~23%; see Table 2, row 16; also Fig. 7). There is an effect of age on the apical angle of the ToC as well (Fig. 7C); whereas the angle is acute (<90°) in adults, the angle is obtuse in newborns, consistent with the flattened appearance of the infant OoC as evident from the mean values presented in Table 2, row 17. Finally, the skewness of the ToC is almost invariably positive, indicating that the tunnel of Corti "leans" towards the modiolus (Fig. 7D). Recall that skew values vary between −1 (apex directly over the foot of the outer pillar cell) and +1 (apex directly over the foot of the inner pillar cell) and a skewness of 0 indicates an equilateral triangle. The infant skew value is significantly closer to 0 than the adult value; hence, the newborn ToC is more symmetrical.

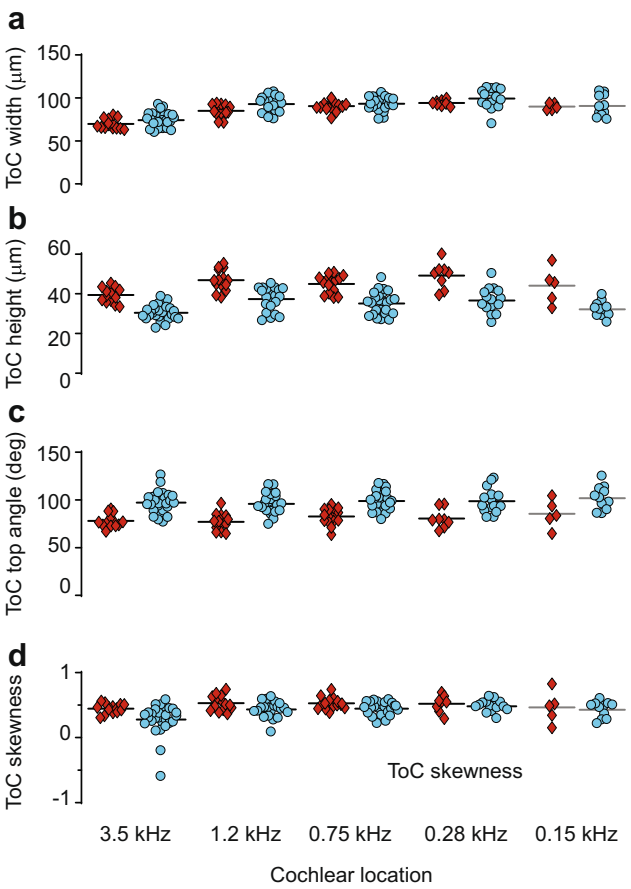

FIG. 7. Shape parameters for the tunnel of Corti. Scatter plots for the four parameters that describe the tunnel of Corti as a triangle. (A) Width at base, (B) height, (C) angle at apex, and (D) skewness. The layout in each panel is the same with adults shown as *red diamonds* and newborns shown as *cyan circles*. Mean values are indicated by horizontal bars. For each of the metrics, the data at 0.15 kHz were excluded from the analysis because of insufficient observations ($N<8$) for the adults. This is indicated by the *gray* horizontal bars

Effects of Cochlear Location

All but two of the morphological metrics vary with cochlear location (see Table 1). A well-established example is the width of the BM, which increases from base to apex in these adult and newborn cases (Fig. 3C) and in all mammals studied thus far (Guild 1927; Wever 1938; Cabezudo 1978). The increase in BM width along the cochlear spiral arises predominantly from the widening of pars pectinata, with only a small contribution from pars tecta (see Fig. 5). Similarly, previous studies have shown that BM thickness in the human cochlea decreases from base to apex (Bhatt et al. 2001), a result reproduced here for both pars tecta and pars pectinata (Fig. 5A, B).

The ossified and non-ossified portions of the human spiral lamina (Fig. 3A, B) also varied in width as a function of cochlear location: whereas the ossified portion decreases in width from base to apex, the non-ossified bridge segment increases. These opposing trends combine so that the total width of the cochlear partition (OSL + bridge + BM) remains constant along the cochlear spiral (Fig. 3D).

The effect of cochlear location on the scala area is easily observed for the scala tympani (Fig. 2D), which decreases in area from cochlear base to apex. For both scala vestibuli and scala media, dependence on cochlear location is less clear (Fig. 2B, C) and appears nonmonotonic. When going from base to apex, the areas alternately increase and decrease in size, resulting in a "zigzag" pattern visible in the scatter plots. Although less obvious, a similar zigzag pattern may also be present in the scatter plots of OoC height and area (Fig. 6C, D). As detailed in the "Discussion" section, this pattern reflects the difference in effective cutting angle for cochlear half-turns on opposite sides of the modiolus.

Summary of Results

Although compression artifacts appear in these temporal-bone preparations, their influence on the data appears uniformly distributed; hence, they do not bias the interpretation of age or cochlear-location effects. In the absence of significant interactions, the analysis reveals a main effect of age (i.e., significant differences between newborns and adults) for all but two metrics. In newborns compared to adults, the areas of scalae vestibuli and tympani are larger, the organ of Corti is smaller and flatter, the BM is wider and thinner, and the non-ossified bridge segment of

the spiral lamina is also wider. Although the newborn cochlea appears fully formed with respect to the structures assessed here, most of these anatomical features continue to mature in a subtle but significant way. Our evidence for continuing maturation contrasts with the dogma that the human cochlea is entirely adult-like by the third trimester. All but two of the metrics also show a significant effect of cochlear location consistent with classic work on cochlear anatomy.

DISCUSSION

In this study, we quantified morphological features of the human cochlear duct to assess potential differences between adults and newborns around the time of birth. Our motivating goal was to determine whether anatomical immaturities could help explain the functional immaturities seen in low-frequency DPOAE phase-gradient delays (Abdala et al. 2011b; Abdala and Dhar 2012). We derived 18 different metrics at several cochlear locations in histological preparations of adult and infant temporal bones and found significant effects of age and cochlear location on most of the metrics.

Nonmonotonic Dependence on Cochlear Location

An important factor influencing the metrics extracted here is the sectioning angle. The temporal bones in this study were cut in the horizontal plane, from dorsal to ventral, using extracochlear landmarks to fine-tune the tissue orientation, such that the final cutting angle through the inner ear is highly stereotyped. The axis around which the upper turns spiral is also in the horizontal plane, slightly tilted such that the apex is medial and inferior to the base (see Fig. 8). Furthermore, the spiral is stretched along its central axis so that the apex is several millimeters anterior to the base. Given this basic geometry, the horizontal plane tends to cut orthogonal to the cochlear half-turns on the medial side of the modiolus and at a more oblique angle on the lateral half-turns. We assume that this systematic alternation in the effective cutting angle on different half-turns along the duct causes the nonmonotonic dependence on cochlear location ("zigzag" pattern) observed in several of the scatter plots (Figs. 2B, C and 6C, D). Our observation that the angle between the spiral lamina and the modiolus exhibits a similar zigzag pattern provides additional support for the existence of a sectioning artifact (Fig. 9).

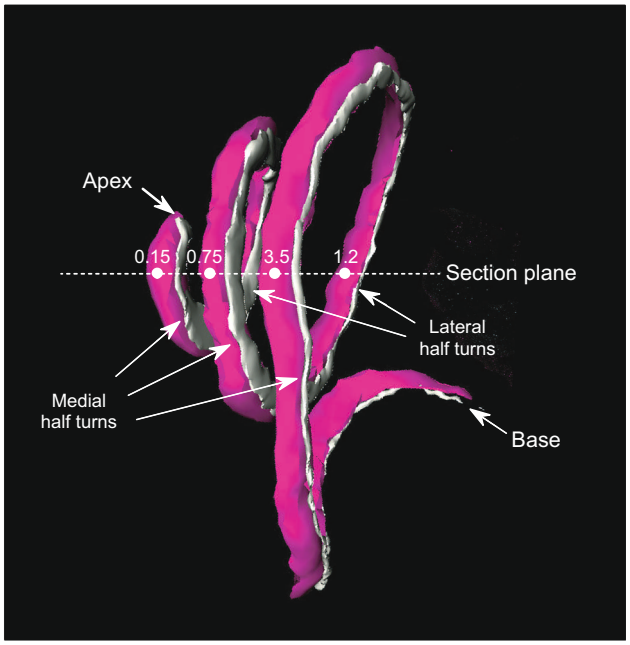

FIG. 8. Temporal-bone model illustrates why sectioning angles differ for lateral vs medial half-turns along the cochlear spiral. The apposed red and white spiraling forms here are extracted from a 3-D model of the human temporal reconstructed from a serial-section set from the MEE collection, prepared identically to the ones studied here (Wang et al. 2006). The red and white surfaces correspond to the scala media and basilar membrane respectively. The frequency correlates of the mid-modiolar sections through several of the half-turns are shown

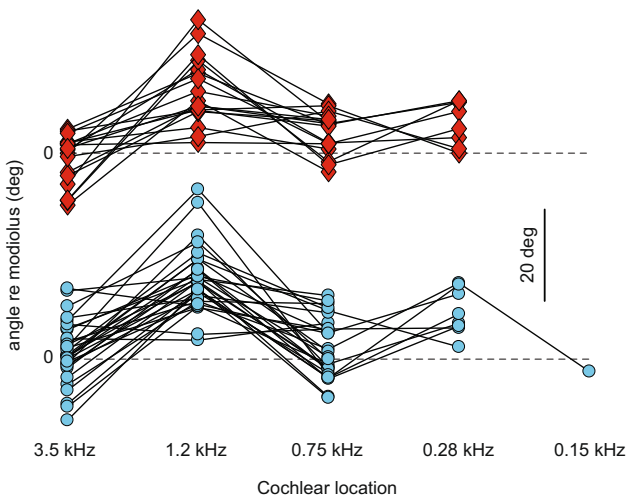

FIG. 9. Angle between spiral lamina and modiolar axis. Scatter plots of the angle between spiral lamina and the modiolar axis for both adults (*red diamonds*) and newborns (*cyan circles*). The angles were measured on the side of scala tympani; values larger than 90° indicate that the spiral lamina "points" towards the apex as viewed from the modiolus. Observations from the same temporal bone are connected by lines. For visual clarity, each age group has an arbitrary vertical offset; the horizontal *gray dashed lines* indicate 90°; the scale bar corresponds to 20°

Morphology of the Newborn Cochlea

Age differences in the shape and size of the organ of Corti are among the most robust effects observed: overall, the newborn OoC is flatter and smaller. This age difference arises because the Hensen-cell region appears to be less highly developed in newborns. Since there is no evidence for postnatal cell proliferation in the sensory epithelium of the mammalian cochlea (e.g., Roberson and Rubel 1994), the eventual maturation of the Hensen-cell region presumably occurs due to an increase in cell size rather than an increase in cell number. However, this speculation cannot be tested with the images and metrics in the present study.

All but two of the metrics reveal an effect of age, indicating that newborn-adult differences extend well beyond the smaller and flatter shape of the neonatal organ of Corti. Although the human cochlea appears structurally complete at birth, and the length of the spiral has reached adult dimensions, many morphological features have yet to attain full maturity, and an ongoing refinement occurs postnatally. Although the residual immaturities cannot always be discerned from measurements at a given cochlear location, a clear pattern emerges from data considered across the cochlear spiral. For example, the total BM (pars tecta + pars pectinata) averages 17.8 μm wider (~6 %) in newborns than in adults (Fig. 3C). This age difference is small compared to the overall width of the BM (range, 175–600 μm) and is less than the variation in BM width at each cochlear location (mean SD = 28.5 μm), making it hard to detect without considering multiple cochlear locations.

Some of the age differences are counter-intuitive. For example, the areas of two of the three scalae are, on average, larger in infants. The origin of this result is unclear; however, developmental changes in the bony canals themselves cannot be ruled out. Bone density and growth are ongoing in the newborn otic capsule beyond the perinatal period (Anson and Bast 1958).

The non-ossified bridge segment of the spiral lamina, and the BM, increases in width from base to apex in both adults and infants, presumably contributing to the progressive decrease in stiffness and resonant frequency from base to apex. However, both the bridge and the BM are wider in newborns throughout the length of the cochlear spiral, resulting in a wider cochlear partition overall. This is consistent with the larger scala area in newborns since the cochlear partition defines a key scalar boundary (Fig. 1a).

Collectively, prior work suggests that the features supporting micromechanical function of the human cochlea are mature by term birth. Yet, no previous study has quantified the architecture of the human cochlea in newborns. Here, we show that, on a scale larger than individual cells and/or organelles, several structural properties are immature in newborns and undergo change after birth. These material and physical features contribute to the mass and stiffness gradients along the length of the cochlear spiral and help establish the frequency-place map. The anatomical immaturities reported here are likely to impact function.

Functional Consequences of Anatomical Immaturities

Many of the anatomical immaturities evident in the newborn cochlea presumably have functional consequences, some of which can be tentatively inferred from conventional conceptions of cochlear macromechanics. For example, both the BM and the adjacent spiral laminar bridge are wider in newborns than in adults, and the BM is thinner. These differences appear throughout the cochlea and suggest that the newborn partition is more compliant. Because transverse waves generally propagate with a speed inversely proportional to the square root of the effective compliance, larger compliance implies slower wave speeds, longer travel times, and greater delays. The observed anatomical differences therefore appear consistent with the longer low-frequency DPOAE phase-gradient delays previously measured in newborns.

Approximating the BM as a uniform rectangular beam (e.g., Olson and Mountain 1991) allows one to estimate the expected ratio of neonatal to adult delays more quantitatively. Taking the delay, τ, proportional to the square root of the volume compliance of the beam yields the relation $\tau_{neo}/\tau_{adult} \approx [(w_{neo}/w_{adult})^5 (d_{adult}/d_{neo})^3]^{1/2}$, where w and d are the BM total width and mean thickness, respectively. All other relevant parameters, including the boundary conditions at the ends of the beam, are assumed unchanged between newborns and adults, and they therefore effectively cancel out. Using the anatomical measurements at the 0.75-kHz location (Table 2, rows 7, 9, and 10) gives the estimate $\tau_{neo}/\tau_{adult} \approx 1.8 \pm 0.6$ (SEM) for comparison with the ratio 1.5 ± 0.1 found for the distortion component of DPOAE delays at the same frequency (Abdala and Dhar 2012). Although surprisingly good, the agreement should be interpreted with caution given the

many simplifying assumptions involved in the calculation, including the omission of possible dynamical effects of the "bridge" (Raufer et al. 2019).

Because low-frequency DPOAE delays in newborns are significantly longer than those in adults, while high-frequency DPOAE delays are similar, we initially hypothesized an immaturity confined to the *apical* half of the newborn cochlea. We were therefore surprised to find anatomical immaturities at both basal and apical cochlear locations studied here. Note, however, that unlike low-frequency DPOAE phase-gradient delays, which may depend at least in part on cochlear travel times, high-frequency phase-gradient delays measured using the fixed-f_2/f_1 DPOAE paradigm are always close to 0 as a result of the local scaling manifest by the basal half of the cochlea (Shera and Guinan 1999). Thus, even if newborn cochlear delays are indeed greater throughout the cochlea, as suggested by their immature anatomy, they may only affect fixed-ratio DPOAE delay measurements at low frequencies. Unfortunately, attempts to work around this limitation by using other types of OAEs (i.e., reflection-source OAEs) to probe neonatal cochlear delays at high frequencies are confounded by the level dependence of these emissions and the immaturities of the neonatal middle ear.

In addition to its effect on traveling-wave delays, a larger compliance of the neonatal cochlear partition would tend to shift the newborn tonotopic map towards lower frequencies compared to the adult. Although the smaller size (and thus mass) of the newborn organ of Corti might naively be expected to offset the greater compliance, perhaps acting to increase local resonant frequencies and shift the map in the opposite direction, any reduction in the volume of vibrating tissue would be countered by a compensating volume of vibrating fluid of almost equal density. Interestingly, any basal-ward shift in the tonotopic map that occurs during maturation due to increasing stiffness may subsequently be reversed during aging: the group delays of stimulus-frequency OAEs are longer in elderly adults, consistent with an age-related decrease in partition stiffness (Abdala et al. 2018).

Despite the macromechanical speculations offered above, the functional consequences of most of the observed anatomical immaturities are difficult to assess without extensive computational modeling in which details of cochlear micromechanics and related material properties are well represented. Good examples include the noted differences in the shape and size of the organ of Corti and the geometry of the tunnel. The measurements reported here, including their variation along the cochlear spiral, provide the necessary empirical foundation for future modeling studies, whether they aim to probe the maturation of cochlear function or understand the mechanical responses of the adult human cochlea.

ACKNOWLEDGMENTS

We thank the anonymous reviewers for their helpful comments on the manuscript.

Funding information This study was supported by grants DC003552 (CA), DC003687 (CAS), and DC0188 (MCL) from the National Institutes of Health.

REFERENCES

Abdala C, Dhar S (2012) Maturation and aging of the human cochlea: a view through the DPOAE looking glass. J Assoc Res Otolaryngol 13:403–421. https://doi.org/10.1007/s10162-012-0319-2

Abdala C, Dhar S, Kalluri R (2011a) Level dependence of distortion product otoacoustic emission phase is attributed to component mixing. J Acoust Soc Am 129:3123–3133. https://doi.org/10.1121/1.3573992

Abdala C, Dhar S, Mishra S (2011b) The breaking of cochlear scaling symmetry in human newborns and adults. J Acoust Soc Am 129:3104–3114. https://doi.org/10.1121/1.3569737

Abdala C, Keefe DH (2012) Morphological and functional ear development. In: Werner L, Fay RR, Popper AN (eds) Springer handbook of auditory research: human auditory development. Springer, New York, pp 19–59

Abdala C, Ortmann AJ, Shera CA (2018) Reflection- and distortion-source otoacoustic emissions: evidence for increased irregularity in the human cochlea during aging. J Assoc Res Otolaryngol 19:493–510. https://doi.org/10.1007/s10162-018-0680-x

Amatuzzi M, Liberman MC, Northrop C (2011) Selective inner hair cell loss in prematurity: a temporal bone study of infants from a neonatal intensive care unit. J Assoc Res Otolaryngol 12:595–604. https://doi.org/10.1007/s10162-011-0273-4

Anson BJ, Bast TH (1958) Development of the otic capsule of the human ear; illustrated in atlas series. Q Bull Northwest Univ Med Sch 32(2):157–172

Bast TH, Anson BJ (1949) The temporal bone and the ear. Charles C. Thomas, Springfield, IL

von Békésy G (1960) Experiments in hearing. McGraw-Hill Book Co, New York

Bhatt KA, Liberman MC, Nadol JB Jr (2001) Morphometric analysis of age-related changes in the human basilar membrane. Ann Otol Rhinol Laryngol 110:1147–1153. https://doi.org/10.1177/000348940111001212

Bredberg G (1968) Cellular pattern and nerve supply of the human organ of Corti. Acta Otolaryngol Suppl 236:1+

Cabezudo LM (1978) The ultrastructure of the basilar membrane in the cat. Acta Oto-Layringol 86:1–6. https://doi.org/10.3109/00016487809124733

DALLOS P (2003) Organ of Corti kinematics. J Assoc Res Otolaryngol 4:416–421. https://doi.org/10.1007/s10162-002-3049-z

EDGE RM, EVANS BM, PEARCE M, RICHTER C-P, HU X, DALLOS P (1998) Morphology of the unfixed cochlea. Hear Res 124:1–16

GREENWOOD DD (1990) A cochlear frequency-position function for several species—29 years later. J Acoust Soc Am 87:2592–2605. https://doi.org/10.1121/1.399052

GUILD SR (1927) The width of the basilar membrane. Science 65:67–69

IGARASHI Y (1980) Cochlear of the human fetus: a scanning electron microscope study. Arch Histol Jap 43:195–209

IGARASHI Y, ISHII T (1980) Embryonic development of the human organ of Corti: electron microscopic study. Int J Pediatr Otorhinolaryngol 2:51–62. https://doi.org/10.1016/0165-5876(80)90028-2

JEFFERY N, SPOOR F (2004) Prenatal growth and development of the modern human labyrinth. J Anat 204:71–92

LAVIGNE-REBILLARD M, PUJOL R (1986) Development of the auditory hair cell surface in human fetuses. A scanning electron microscopy study. Anat Embryol (Berl) 174:369–377

LAVIGNE-REBILLARD M, PUJOL R (1987) Surface aspects of the developing human organ of Corti. Acta Otolaryngol Suppl:436: 43–436: 50

LAVIGNE-REBILLARD M, PUJOL R (1988) Hair cell innervation in the fetal human cochlea. Acta Otolaryngol 105:398–402

LAVIGNE-REBILLARD M, BAGGER-SJÖBÄCK D (1992) Development of the human stria vascularis. Hear Res 64:39–51. https://doi.org/10.1016/0378-5955(92)90166-K

LIM DJ, RUEDA J (1992) Structural development of the cochlea. In: Romand R (ed) Development of auditory and vestibular systems 2, Elsevier, Amsterdam, pp 33–58

LIM R, BRICHTA AM (2016) Anatomical and physiological development of the human inner ear. Hear Res 338:9–21. https://doi.org/10.1016/j.heares.2016.02.004

MAKARY CA, SHIN J, KUJAWA SG, LIBERMAN MC, MERCHANT SN (2011) Age-related primary cochlear neuronal degeneration in human temporal bones. J Assoc Res Otolaryngol 12:711–717. https://doi.org/10.1007/s10162-011-0283-2

MERCHANT SN, NADOL JB (2010) Schuknecht's pathology of the ear, 3rd edn. People's Medical Publishing House-USA, Shelton, CT

OLSON ES, MOUNTAIN DC (1991) In vivo measurement of basilar-membrane stiffness. J Acoust Soc Am 89:1262–1275. https://doi.org/10.1121/1.400535

PREIBISCH S, SAALFELD S, TOMANCAK P (2009) Globally optimal stitching of tiled 3D microscopic image acquisitions. Bioinformatics 25:1463–1465. https://doi.org/10.1093/bioinformatics/btp184

PUJOL R (1985) Morphology, synaptology and electrophysiology of the developing cochlea. Acta Otolaryngol Suppl 421:5–9

PUJOL R, HILDING D (1973) Anatomy and physiology of the onset of auditory function. Acta Otolaryngol 76:1–10

PUJOL R, LAVIGNE-REBILLARD M (1985) Early stages of innervation and sensory cell differentiation in the human fetal organ of Corti. Acta Otolaryngol Suppl 423:43–50

RAUFER S, CHO NH, GUINAN JJ, PURIA S, NAKAJIMA HH (2019) The anatomy and cochlear partition motion-pattern of the human is different from those of laboratory animals: optical coherence tomography (OCT) measurements. Assoc Res Otolaryngol Abs 42:95–96

RETZIUS G (1884) Das Gehörorgan der Wirbelthiere. Morphologisch-histologische Studien. Band II. Das Gehörorgan der Reptilien, der Vögel und der Säugethiere. Samson and Wallin, Stockholm, Sweden

ROBERSON DW, RUBEL EW (1994) Cell division in the gerbil cochlea after acoustic trauma. Am J Otolaryngol 15:28–34

RUBEN RJ (1967) Development of the inner of the mouse: a radioautographic study of terminal mitosis. Acta Otolaryngol Suppl 220:1–44

SÁNCHEZ-FERNÁNDEZ JM, RIVERA JM, MACIAS JA (1983) Early aspects of human cochlea development and tectorial membrane histogenesis. Acta Otolaryngol 95:460–469

SCHINDELIN J, ARGANDA-CARRERAS I, FRISE E, KAYNIG V, LONGAIR M, PIETZSCH T, PREIBISCH S, RUEDEN C, SAALFELD S, SCHMID B, TINEVEZ JY, WHITE DJ, HARTENSTEIN V, ELICEIRI K, TOMANCAK P, CARDONA A (2012) Fiji: an open-source platform for biological-image analysis. Nat Methods 9:676–682. https://doi.org/10.1038/nmeth.2019

SHERA CA, GUINAN JJ (1999) Evoked otoacoustic emissions arise by two fundamentally different mechanisms: a taxonomy for mammalian otoacoustic emissions. J Acoust Soc Am 105:782–798. https://doi.org/10.1121/1.426948

SHERA CA, TALMADGE CL, TUBIS A (2000) Interrelations among distortion-product phase-gradient delays: their connection to scaling symmetry and its breaking. J Acoust Soc Am 108:2933–2948. https://doi.org/10.1121/1.1323234

TANAKA K, SAKAI N, TERAYAMA Y (1979) Organ of Corti in the human fetus: scanning and transmission electronmicroscope studies. Ann Otol Rhinol Laryngol 88:749–758. https://doi.org/10.1177/000348947908800602

TASAKI I, DAVIS H, ELDREDGE DH (1954) Exploration of cochlear potentials in Guinea pig with a microelectrode. J Acoust Soc Am 26:765–773. https://doi.org/10.1121/1.1907415

TEMCHIN AN, RICH NC, RUGGERO MA (2008) Threshold tuning curves of chinchilla auditory-nerve fibers. I. Dependence on characteristic frequency and relation to the magnitudes of cochlear vibrations. J Neurophysiol 100:2889–2898. https://doi.org/10.1152/jn.90637

WANG H, NORTHROP CC, BURGESS B, LIBERMAN MC, MERCHANT SN (2006) Three-dimensional virtual model of the human temporal bone: a stand-alone, downloadable teaching tool. Otol Neurotol 27:452–457

WEVER ER (1938) The width of the basilar membrane in man. Ann Otol Rhinol Laryngol 47:37–47. https://doi.org/10.1177/000348943804700102

ZWEIG G (1976) Basilar membrane motion. Cold Spring Harb Symp Quant Biol 40:619–633